

High Intensity Focused Ultrasound Catheter Dosimetry using Gel Phantom.

by

Yegor D. SineInikov^{1*}, Oleg Y. Polyakov², Oleg A. Sapozhnikov³,
Jaime E. Merino¹, Dmitry Mayorov¹, and Eugene Jung¹

¹ ProRhythm, 105 Comac St, Ronkonkoma, NY 11779, USA

² Columbia University, Physics Department, New York, NY 10027, USA.

³ Moscow State University, Physics Department, Moscow 119992, Russia.

Submitted to

Ultrasonic Industrial Association

March 2006

Presented as Invited Paper at the Ultrasonic Industrial Association

35th Symposium

Coronado Island Marriott Resort,

San Diego, CA USA

14 March 2006

* Corresponding Author (to whom all correspondence should be addressed)

Introduction.

Atrial fibrillation (AF) is the most common sustained cardiac arrhythmia identified as a leading risk factor for stroke afflicting about two million people in United States and more than four million worldwide. Recently, it has been demonstrated that AF originates in pulmonary veins (PV) [1] and that ablation or isolation of PV markedly reduces episodes of AF. One of the most effective way for PV ablation is application of High Intensity Focused Ultrasound (HIFU). The ProRhythm has designed the HIFU PV ablation System to create a circumferential lesion in the left atrium surrounding the ostium to electrically isolate the problematic PVs. This paper describes the design of the catheter and focuses on the thermal dose characterization using gel phantom.

AF Ablation Background.

With the aging of the population in industrial countries the rise in the prevalence of AF becomes a major health concern. A patient with AF is more likely to have a stroke than the general population. This created an enormous backlog of individuals who would be treated if an effective and simple procedure were developed.

One of the earliest alternatives to both cardioversion and standard pharmacological therapy was the surgical maze procedure [2]. Later catheter based AF ablation became the prime focus of many electrophysiologists around the world, spawning numerous variations ranging from “fire” [3] to “ice” [4]. For a number of reasons, ultrasonic methods [e.g. 5, 6] appear to be at the forefront of this new breed of catheter based AF ablation techniques. Ultrasonic therapeutic devices are not required to maintain tight contact with the target tissue in order to create a lesion. Ultrasound can be aimed in many directions at once, eliminating the need for the time consuming point-by-point work. The ability to direct high intensity energy at depth, without relying on thermal conduction, drastically widens the window between transmural lesion formation and potentially life-threatening steam-pop, charring, and other thrombogenic surface effects. All of these advantages make ultrasound, not only a potentially safer energy delivery modality for cardiac ablation, but also a procedurally simpler modality as well.

HIFU Catheter Operation Principle.

The PRI device uses a uniquely shaped balloon that provides a positive, fluoroscopically visible mate to the ostia of the pulmonary vein, ensuring rapid and proper positioning of the intended lesion. Specially constructed proprietary designed catheter, allows delivery of water flow, gas inlet, electrical connection, and steering.

The distal end of the catheter is equipped with inner and outer balloon structure. During sonication, the inner balloon is fully inflated to rigid. Balloon parabolic reflective interface created by means of secondary gas filled outer balloon redirects and focuses the radiation from

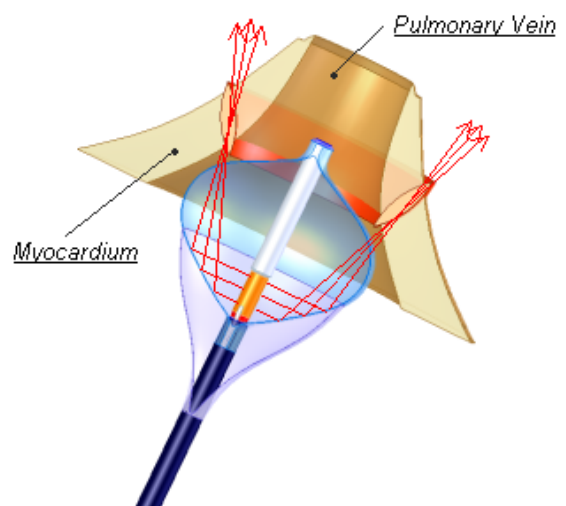


Figure 1. Operating principle of PRI HIFU catheter to create circumferential lesion around pulmonary veins.

the cylindrical transducer into an annular region of extremely high acoustic intensity within the ostial tissue surrounding a chosen pulmonary vein, as shown on Figure 1.

PRI catheters are typically characterized using power balance measurements and hydrophone beam profile evaluation. Hydrophone maps are used to assess the uniformity of the transducer and focal directivity. The catheter acoustic performance specifications are summarized below.

Table 1. HIFU PV Catheter Acoustic Performance

Specified Acoustic Output	32 Watts nominal power
Specified Input	100 Watts
Acoustic intensity	200 - 300 W/cm ²
Transducer Surface Area	60 mm ²
Nominal Operating Frequency	9 MHz
Thermal Dosage	40 – 90 sec
Total Irradiated Energy	1280 –2280 J
Power Delivery Regime	Continuous wave
Beam Shape	Annular ring

Acoustic Field Modeling

The acoustic field and thermal simulation provides a design guidance and guides data analysis. The acoustic focal field patterns were calculated in two steps. First, we followed the approach described in paper [7] in order to obtain complex acoustic pressure at balloon reflective interface. By taking Fourier transform and solving differential equation, the desired expression for the acoustic pressure amplitude at a given observation point (r, z) is:

$$p'(r, z) = -i \frac{2\Omega\rho_0c_0v_0}{\pi} \int_0^{+\infty} \frac{\sin \xi}{\xi} \cdot \frac{H_0^{(1)}\left(\sqrt{\Omega^2 - \xi^2} \cdot \frac{2r}{h}\right)}{\sqrt{\Omega^2 - \xi^2} \cdot H_1^{(1)}\left(\sqrt{\Omega^2 - \xi^2} \cdot \frac{2a}{h}\right)} \cdot \cos\left[\left(\frac{2z}{h} - 1\right)\xi\right] d\xi \quad (1)$$

where Ω is a dimensionless frequency $\Omega = \frac{\omega h}{2c_0}$, $\xi = k_z h/2$, $k = \omega/c$ is wavenumber, h is transducer height, a is transducer radius, v_0 is complex amplitude of transducer surface velocity. $H_0^{(1)}(\zeta)$ is Hankel functions of the 1st kind. Second, we solved the radiation problem by placing acoustic sources on reflective interface. The acoustic pressure of the corresponding source is simply an inversion of the incident pressure, to maintain zero pressure balance. The final acoustic field is calculated numerically on the base of the 2nd Rayleigh integral:

$$P(r, \psi, z) = \frac{1}{2\pi} \int_S P(r', \psi', z') \frac{\partial}{\partial n} \left(\frac{e^{ikR}}{R} \right) dS' \quad (2)$$

Here cylindrical coordinates (r, ψ, z) correspond to an observation point, (r', ψ', z') correspond to a point on the reflecting surface, \mathbf{n} is a unit normal to the reflecting surface, R is distance between the points (r, ψ, z) and (r', ψ', z') . Note that equation (2) represents exact solution only in plane wave case. However, it is applicable because the curvature radius of the reflective surface is much bigger than the wavelength. Focal acoustic field were calculated for different balloon and transducer configurations. In general there is an excellent agreement between calculated and hydrophone measured acoustic data. The maximum acoustic pressure was estimated on the order of 3 MPa, while hydrophone yielded 1.7 (0.8) MPa. Typical transmural acoustic field directivity pattern is shown on Figure 2.

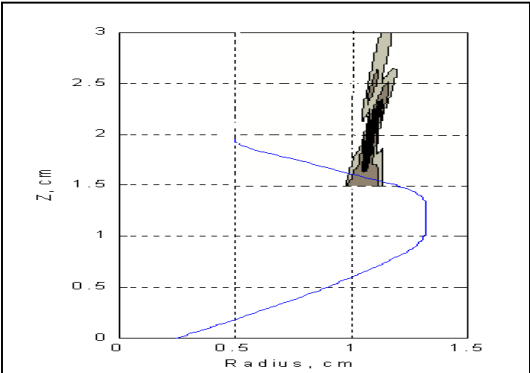


Figure 2. Calculated acoustic field.

Thermal Simulation

Using calculated acoustic intensities the lesion growth is simulated by solving Bio-Heat-Transfer Equation

$$\rho_t c_t \frac{\partial T}{\partial t} = k \nabla^2 T - w_b c_b (T - T_b) + \eta_t I \tag{3}$$

where ρ_t is the density of the tissue, c_t is the specific heat of the tissue, T is the temperature of the tissue, t is the time, w_b is the blood perfusion rate, c_b is the specific heat of the blood, T_b is the arterial blood temperature, k is the thermal conductivity of the tissue, η_t is the absorption of the tissue, I is the intensity of the ultrasound field that depends on attenuation in the tissue, the power of the transducer and the geometry of the problem. Equation (3) was solved using Crank-Nicholson second order accurate in time differencing scheme to determine acoustic power – lesion formation time relationships to guide interpretation of experimental data. The concept of thermal dose was used to transform the temperature exposure over time into the tissue damage [8]. The simulations were performed on idealized model of ostia using tissue parameters summarized in Table 2.

Table 2. Parameters used in computer simulations.

Parameter	Value
Attenuation, absorption coefficient	13 Nepers/m/MHz
Tissue density	1060 kg/m ³
Thermal conductivity	0.5 W/m/C
Blood perfusion	13.5 kg/m ³ /s
Specific heat of tissue	3720 J/kg/C
Specific heat of blood	3770 J/kg/C

The temperature was calculated over sufficiently large transmural region assuming zero thermal flux normal to the plane of interest. Defined by thermal dose, lesion formation simulations were performed over various grids using adiabatic and isothermal boundary conditions, as shown on Figure 3. The events of lesion temperature elevating by 15°C, and lesion reaching 3 mm depth were recorded during simulation. Input acoustic power varied from 20 to 50 W. Analytical expression of lesion event formation as a function of time and power was derived from simulation data. For convenience of interpretation, the reference power, P_a at electrical 100 W was assumed equal to 37 W, which is an average acoustic power for experimental catheters at 100 W electrical. Thus, the lesion formation time, T_f , is proportional to the exponent of applied acoustic power, P_a and is described by following formulae:

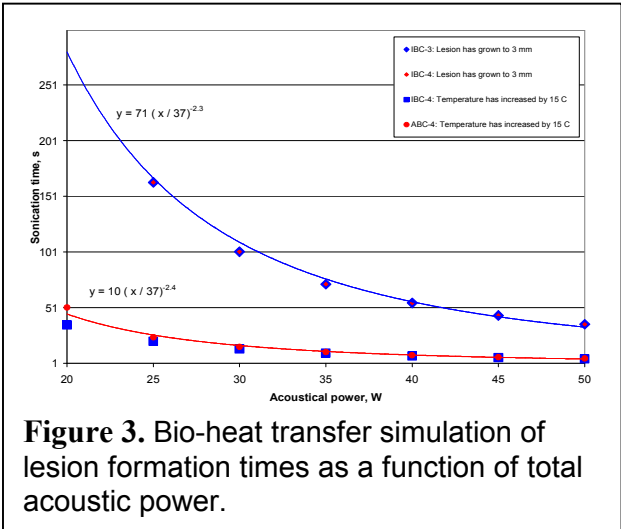


Figure 3. Bio-heat transfer simulation of lesion formation times as a function of total acoustic power.

$$T_f = \tau * (P_a / P_{a \text{ at electrical } 100 \text{ W}})^{-2.3} \quad (4)$$

Where τ is the time it takes to reach a specific lesion formation event at 100 W input electrical power. The larger this proportionality constant, the longer ablation is required to make a lesion. The smaller it is, the faster the ablation can be performed. For example, if two population of data are found to have τ_1 and τ_2 where $\tau_1 > \tau_2$, then at any acoustic power the ablation will be longer for population with larger τ_1 , and shorter for the population with τ_2 .

Dosing Experiments

Treatment planning, namely thermal dose characterization is an important step defining the success of focused ultrasound therapy. Definition of thermal dose incorporates a range of experimental and theoretical studies. Certain deficiencies of *in-vivo* experiments, such as canine thigh studies [9], arise from the complexity and variability of the medium. Consequently, we employ experiments using polyacrylamide phantom material [10] that admit the precise control of various acoustic parameters, and allows precise *in-situ* monitoring of lesion formation. Gel phantom simulates both the acoustical properties and thermal properties of human tissue. It is also optically clear and turns white when temperature reaches 70°C in course of active ultrasound power deposition, thus becoming an ideal

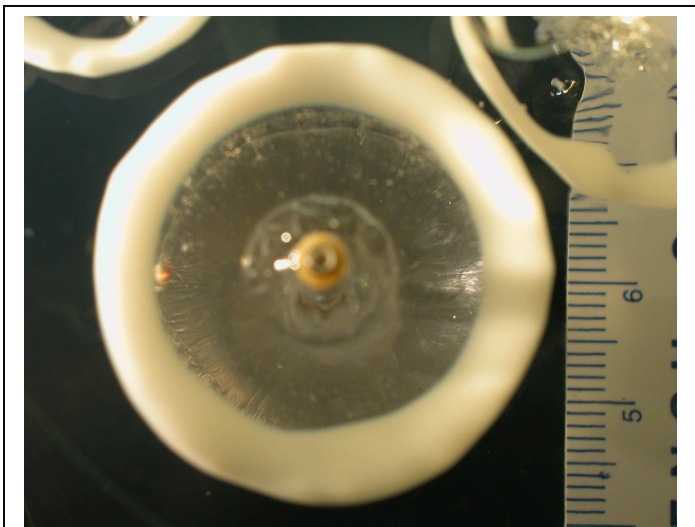


Figure 4. Lesions in polyacrylamide gel (front view).

media for accurate lesion formation characterization. An example of circumferential lesion in gel using PRI HIFU catheter is shown on Figure 4.

Experimental data was analyzed using equation (4). It provided a consistent way of describing lesion formation process as a function of applied power, contained by single parameter to fit. That single parameter, a proportionality constant τ , called below as characteristic time, was obtained for three lesion formation events and catheter sizes discussed below. Two approaches were employed in data analysis: in first, all catheters were treated disrespectful to their size. In second, differential approach, catheters of each size were investigated to obtain individual coefficients and detect differences otherwise hidden in the noise of data.

Nucleation time was defined as the first visual appearance of the opaqueness in the gel. Nucleation times were easy to detect and thus constituted the most accurate data set compared to subsequent events. For acoustic powers greater than 25 W (about 70 W electrical), the nucleation time remained relatively stable around 6-7 seconds and linear with respect to acoustic power. For lower powers, the nucleation time exponentially increased as power decreased. This change in lesion formation is associated with a regime change from active power deposition above 25 W to thermal conduction regime below. At low powers, some intra-size catheter differences also become more apparent, but still difficult to resolve because of the large variation in data. First approach yielded characteristic nucleation time of 5.65 ± 1.78 seconds. Catheters followed the same nucleation curve with small spread, and could be used to predict accurate overall catheter trend in nucleation time as a function of acoustic power. Differential approach provided characteristic nucleation times for each catheter size, listed in Table 3. Detectable upward trend in characteristic nucleation times as the catheter size increases is shown on Figure 5.

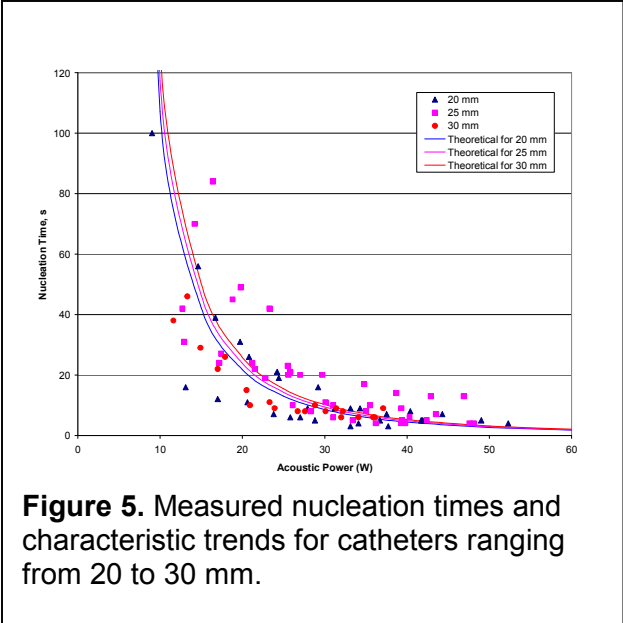


Figure 5. Measured nucleation times and characteristic trends for catheters ranging from 20 to 30 mm.

Closed circle time was defined as a visual closure of the lesion around the balloon. It typically required operator interpretation and careful observation of last visual bridging of the lesion. This data set has therefore larger operator dependent error, and the data are more scattered than nucleation times discussed above. The closed circle time clearly shows an inverse relationship with respect to acoustic power, compatible with equation (4) formalism. At powers of 25 W and greater the closed circle time remains relatively stable for each catheter. At lower powers the differences between uniform and non-uniform catheters immerge. In both

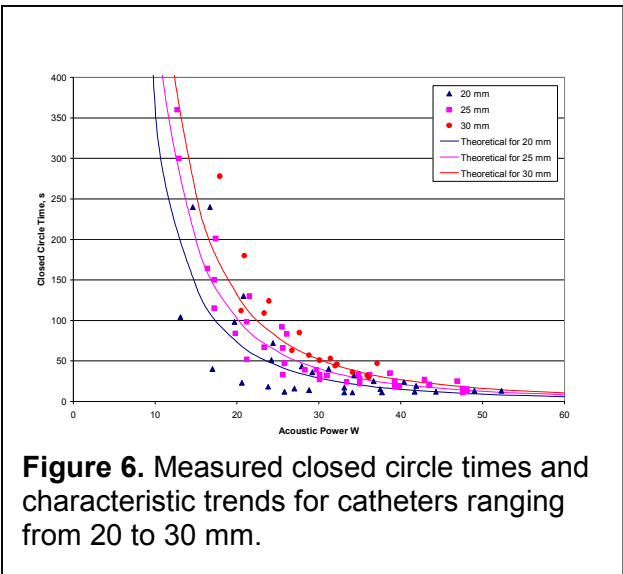


Figure 6. Measured closed circle times and characteristic trends for catheters ranging from 20 to 30 mm.

of these groups we notice that smaller size catheter has lower closed circle time. This is consistent with the fact that smaller catheters have typically higher power output and thus smaller ablation time. First approach yielded characteristic closed circle time of 23.60 ± 6.34 seconds. Differential approach provided characteristic closed circle times for each catheter size, listed in Table 3. Figure 6 shows the size differentiated experimental closed circle times and theoretical curves.

The behavior of 4mm depth time versus acoustic power is similar to the described above. The 4 mm depth time was measured by monitoring lesion formation until it reaches 4 mm depth all around the balloon by visually comparing lesion depth to balloon tip. Large uncertainty, up to 25%, can be attributed to this data set because of the difficulty of visual interpretation. This 4 mm depth time followed the general trends as described above. At powers greater than 30 W the time remains relatively stable and at lower powers it begins to differ greatly. The smaller catheters generally performed better than the larger catheters. Characteristic 4 mm depth time of 36.43 ± 7.39 seconds (see Table 2) was obtained for all catheters. Characteristic 4 mm depth times for each catheter size are listed in Table 3. Figure 7 shows experimental 4 mm depth times with respective theoretical results. Characteristic 4 mm depth circle times are consistent with measurements and allow explicit detection of catheter size dependent differences.

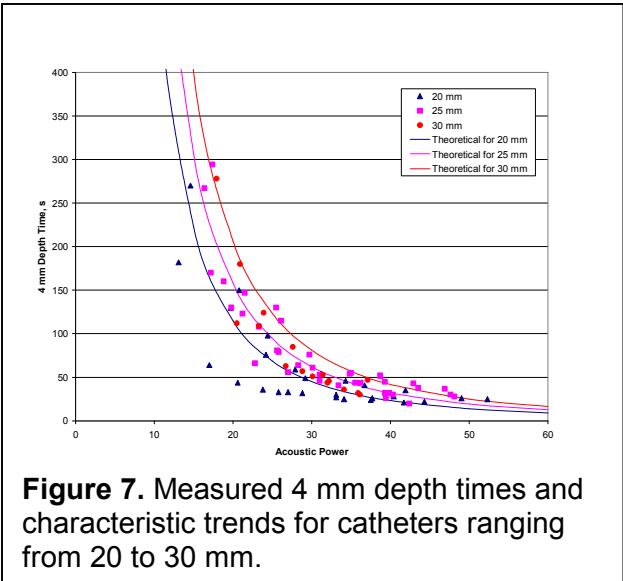


Figure 7. Measured 4 mm depth times and characteristic trends for catheters ranging from 20 to 30 mm.

Table 3. Characteristic lesion formation times in seconds.

Type	Nucleation time	Closed Circle	4 mm Depth
All sizes	5.65 ± 1.78	23.60 ± 6.34	36.43 ± 7.39
20 mm	5.22 ± 1.10	17.63 ± 3.72	27.55 ± 6.08
25 mm	5.72 ± 1.78	24.65 ± 6.49	37.93 ± 8.45
30 mm	6.2 ± 1.90	31.71 ± 9.98	49.52 ± 7.24

Catheter Uniformity

The uncertainty in the measurements also comes from the variation in circumferential uniformity of catheters. Uniformity is characterized by simulated ablation time obtained from two-dimensional azimuthal data collected over 360°. Acquired hydrophone raw data are averaged over radius and processed using single-dimensional bio-heat transfer equation simulation. The results are compared on a relative scale to a perfectly uniform field. The later yields ablation time of 33 simulated seconds.

Ten catheters of different hydrophone characterized uniformity were selected. Catheters with uniformity above 80 seconds clearly show larger depth penetration and longer lesion closure

times. The lesion formation events were found to be both acoustic power and uniformity dependent. Two-dimensional plots were created to investigate the effect of these parameters, as shown on Figure 8. The resolution of the plots is limited by available data. The values for which there was no data are marked by x.

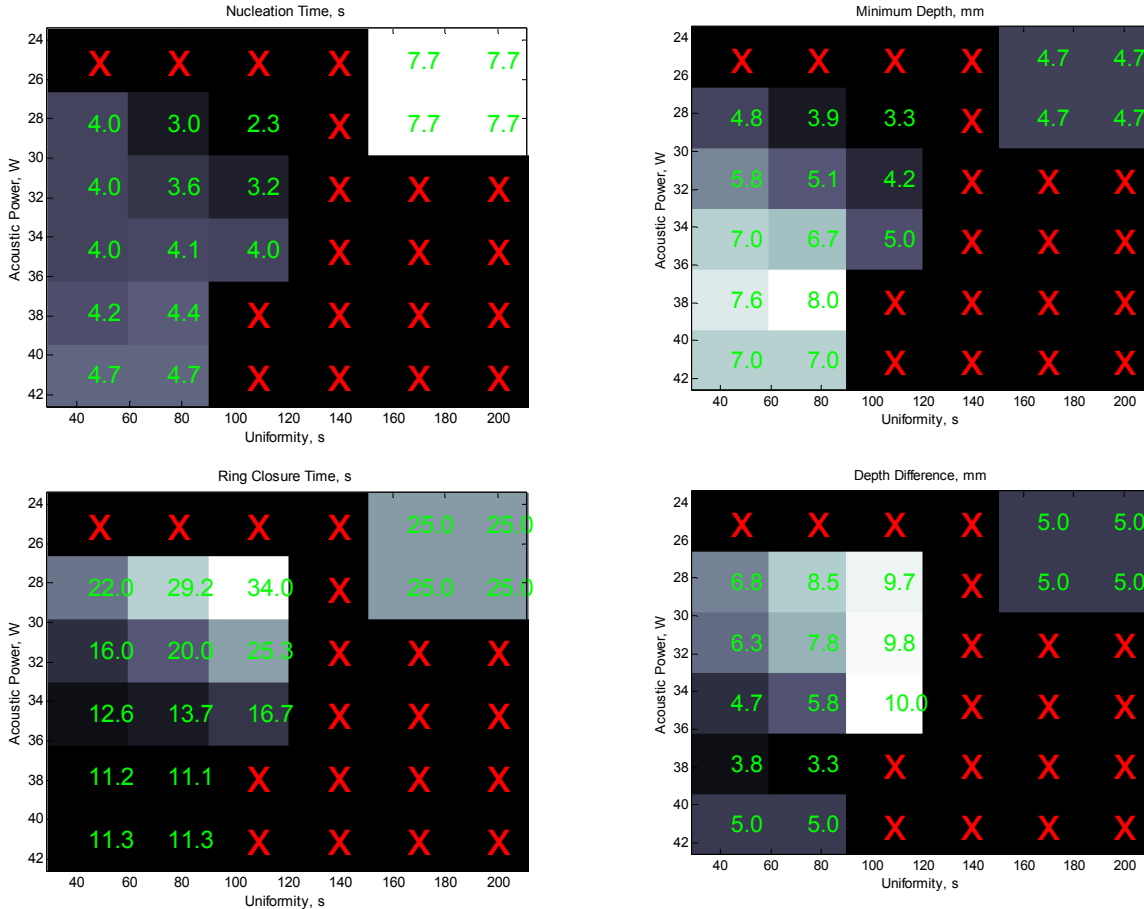


Figure 8. Lesion nucleation (top) and closed circle (bottom) times of 20 mm catheter as a function of uniformity and acoustic power. Minimum lesion depth (top) and depth difference between maximum and minimum (bottom) of 20 mm catheter as a function of uniformity and acoustic power.

Analyzing the above graphs the following observations can be made: nucleation time increases with acoustic power and decreases with catheter uniformity time. This implies that low power non-uniform catheters will have smaller nucleation time than high power uniform catheters. Lesion closure time decreases as acoustic power increases, and it increases with uniformity time. Not surprisingly, this indicates that high acoustic power uniform catheters have shorter lesion closer time. The minimum and maximum lesion depth were measured at the end of sonication at recommended dosage settings. Minimum lesion depth is larger for high power uniform catheters. Minimum lesion depth tends to decrease as acoustic power decreases and as catheter uniformity becomes worse. The difference between maximum and minimum depth decreases as acoustic power increases and catheters uniformity improves, with exception of one catheter. The difference between lesion maximum and minimum depth is also smaller for uniform catheters with acoustic power below 40 Watts. Single catheter with high acoustic power resulted in lesion with larger depth variation than its lower power

counterparts. This could be a result of non-linear absorption, or an artifact of ablation in gel, and more data are needed to understand this effect.

Discussion

Gel ablations results are consistent with simulation and *in-vivo* canine thigh tests [reported elsewhere]. The results show that PRI catheter is able to produce 6 – 12 mm deep circumferential transmural lesions. Within uncertainty of the measurements, any size catheter thermal efficacy is a function of output acoustic power, well described by equation (4). Thermal efficacy of catheters is roughly linear with respect to acoustic power above 30 Watts. In this regime, thermal conduction is superseded by active ultrasound heating. Thus, small variation of input power does not require a change in ablation time. Ablation time and power predictions are consistent when derived from closed circle and 4 mm depth characteristic times. Nucleation time prediction differs from both closed circle and 4 mm depth by showing better match between catheters of different size. Because nucleation time is sensitive primarily to the acoustic intensity rather than total power, it is least favorable method of characterizing long-term lesion formation. Instead, closed circle, and 4 mm depth formation events take into account long term thermal diffusion effects and yield consistent prediction of required power and ablation time for catheter of different sizes.

Catheters circumferential uniformity is the second major factor affecting its ablative performance. Data show clear correlation between the times of lesion formation and catheter uniformity. Non-uniform catheters require substantially larger power or ablation time to achieve the same thermal efficacy. The danger of producing a collateral damage to the deep underlying tissues is recognized for non-uniform catheters, and tight control of catheter and transducer uniformity is in place.

Conclusion

The results of lesion formation in gel complement *in-vivo* canine thigh data. Good agreement is observed between derived dosing parameters, laboratory gel studies, canine thigh studies, theoretical predictions, and up-to-date clinical experience. By utilizing the trends deduced from thermal modeling and evaluating lesion formation in gel it was possible to establish dosing parameters for various balloon sizes with great confidence.

Acknowledgements

We would like to extend our gratitude to Dr. Peter Kaczkowski for his help with polyacrylamide gel identification and processes. This paper was written while the corresponding author (YDS) was an employee at ProRhythm; he thanks Reinhard Warnking and all participating staff for their support.

References

1. Jais P, Haissaguerre M, Shah DC, 1997, A focal source of atrial fibrillation treated by discrete radio frequency ablation. , *Circulation*, 95, 572-576;
2. Cox J, Canavan T, and Schusasler R, 1991, The Surgical Treatment of Atrial Fibrillation II: Intraoperative Electrophysiologic Mapping and Description of the Electrophysiologic Basis of Atrial Flutter and Atrial Fibrillation, *Thorac. Cardiovascular Surg.*, 101, 406-426;

3. Keane D, Reddy V., Ruskin J, 2005, Emerging Concepts on Catheter Ablation of Atrial Fibrillation from the Tenth Annual Boston Atrial Fibrillation Symposium, *Journal of Cardiovascular Electrophysiology*, 16, 9, 1025-1028;
4. Tse H.-F., Sin P.-Y., Siu C.-W., Tsang V., Lam C.L.K., Lau C.-P., 2005, Successful Pulmonary Vein Isolation Using Transvenous Catheter Cryoablation Improves Quality-of-Life in Patients with Atrial Fibrillation, *PACE*, 28, , 421-424;
5. Bailey MR, Khokhlova VA, Sapozhnikov OA, Kargl SG, Crum LA, 2003, Physical mechanisms of the therapeutic effects of ultrasound (A review), *Acoustical Physics*, 49, 4, 369-388;
6. Cathingol D, 2002, High intensity piezoelectric sources for medical applications: technical aspects, *Nonlin. Acoustics at the Beginning of 21st Century*, ed. by Rudenko OV and Sapozhnikov OA, 1, , 371-378;
7. Alekseev VK and Lependin LF, 1967, Acoustic field of a pulsating ring on a cylinder, *Akusticheskii Zhurnal*, 14, 4, 126;
8. Hynynen K, Dennie J, Zimmer J, Simmons W, He DS, Marcus F, and Aguirre M, 1997, Cylindrical Ultrasonic Transducers for Cardiac Catheter Ablation, *IEEE Trans. Biomedical Engineering*, 44, 2, 144-151;
9. Nakagawa H, Yamanashi WS, Pitha JV, Arruda M, Wang X, Otomo K, Beckman KJ, McClelland JH, Lazzara R, Jackman WM, 1995, Comparison of in vivo tissue temperature profile and lesion geometry for radiofrequency ablation with a saline-irrigated electrode versus temperature control in a canine thigh muscle preparation., *Circulation*, 91, , 2264-2273;
10. Howard S., Yuen J., Wegner P., Zanelli C.I., 2003, Characterization and FEA Simulation for a HIFU Phantom Material, Onda Corp. report;